A priori and a posteriori analysis of the flow around a rectangular cylinder

IOP Conf. Series: Journal of Physics: Conf. Series **923** (2017) 012028 doi:10.1088/1742-6596/923/1/012028

A priori and a posteriori analysis of the flow around a rectangular cylinder

A Cimarelli[1,2], A Leonforte[2], M Franciolini[1], E De Angelis[3], D Angeli[2] and A Crivellini[1]

[1] DIISM, Università Politecnica delle Marche, Via Brecce Bianche, 60131 Ancona, Italy
[2] DISMI, Università di Modena e Reggio Emilia, Via Amendola, 42122 Reggio Emilia, Italy
[3] School of Engineering, Cardiff University, Cardiff CF24 3AA, UK

E-mail: a.cimarelli@staff.univpm.it

Abstract. The definition of a correct mesh resolution and modelling approach for the Large Eddy Simulation (LES) of the flow around a rectangular cylinder is recognized to be a rather elusive problem as shown by the large scatter of LES results present in the literature. In the present work, we aim at assessing this issue by performing an *a priori* analysis of Direct Numerical Simulation (DNS) data of the flow. This approach allows us to measure the ability of the LES field on reproducing the main flow features as a function of the resolution employed. Based on these results, we define a mesh resolution which maximize the opposite needs of reducing the computational costs and of adequately resolving the flow dynamics. The effectiveness of the resolution method proposed is then verified by means of an *a posteriori* analysis of actual LES data obtained by means of the implicit LES approach given by the numerical properties of the Discontinuous Galerkin spatial discretization technique. The present work represents a first step towards *a best practice* for LES of separating and reattaching flows.

1. Introduction

In Large Eddy Simulation (LES) the large scales of the flow are directly computed while leaving to the subgrid stresses the duty of accounting for the small unresolved scales. Three main elements determine the success of the LES approach: (i) the mesh resolution, (ii) the model for the subgrid stresses and (iii) the numerical scheme. These three aspects are inherently related each other so that a certain turbulence model is well suited for a given mesh resolution and numerical algorithm and not for others [1]. For this reason it is often difficult to find out a best practice for LES. An instructive example of the complexity of the LES approach is given by the flow around a rectangular cylinder. As shown in the BARC project (Benchmark on the Aerodynamics of a Rectangular 5:1 Cylinder), see Bruno et al. [2] and references therein, a large scatter of LES results is present even for very simple statistical quantities. One possible explanation is given by the fact that a clear picture of the combined influence of mesh resolution, turbulence model and numerical scheme on the flow statistics is still missing. In this contribution, we aim at assessing the filtered behaviour of the flow, by analysing for the first time filtered Direct Numerical Simulation (DNS) data of such a system. In particular, in this preliminary work, we aim at assessing the role of the mesh resolution on capturing the main flow features. And, hence, we do not consider the possible coupling of the present results with the modelling approach adopted to represent the stresses at subgrid levels. Finally, we perform an actual LES

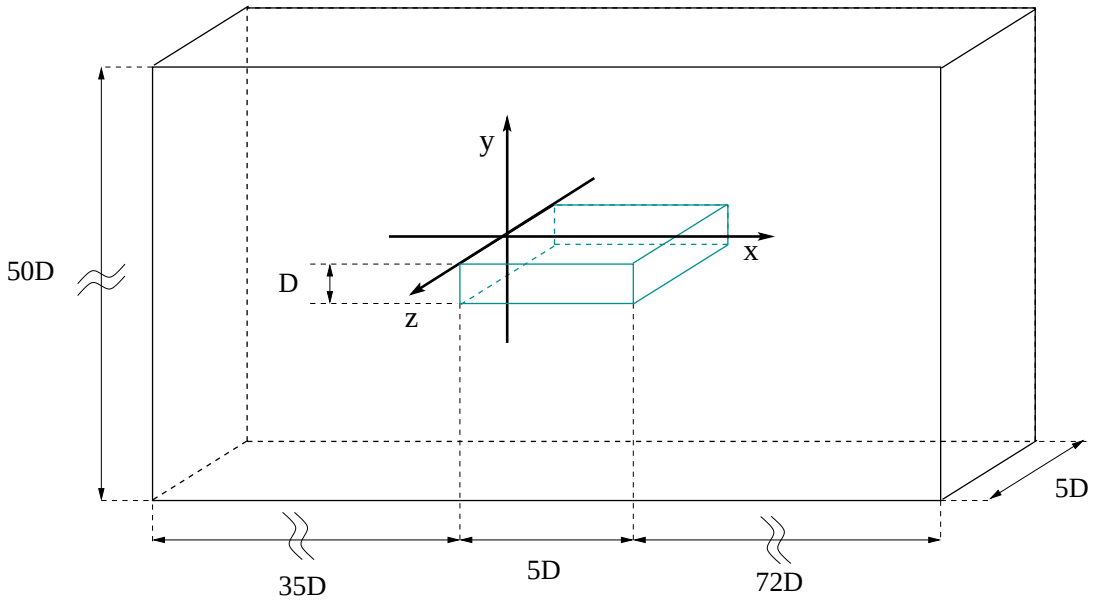

Figure 1. Configuration of the system.

simulation by means of Discontinuous Galerkin (DG) numerical approach in order to prove the results from the DNS.

2. Direct Numerical Simulation

A common practice for the assessment of the behaviour of the resolved field in LES as a function of the filter length employed is to analyse filtered DNS data, the so-called *a priori* analysis. The governing equation numerically integrated when performing a DNS are

$$\begin{aligned} &\frac{\partial u_i}{\partial x_i} = 0 \\ &\frac{\partial u_i}{\partial t} + \frac{\partial u_i u_j}{\partial x_j} = -\frac{\partial p}{\partial x_i} + \frac{1}{Re}\frac{\partial^2 u_i}{\partial x_j \partial x_j} \end{aligned} \tag{1}$$

where $x = x_1$ ($u = u_1$), $y = x_2$ ($v = u_2$), $z = x_3$ ($w = u_3$) are the streamwise, vertical and spanwise directions (velocities), p is the pressure field, and $Re = U_\infty D/\nu$ is the Reynolds number with ν the kinematic viscosity, U_∞ the free-stream velocity and D the rectangle thickness. Unless specifically stated, all the quantities will be reported in a dimensionless form by using D and U_∞ for the lengths and velocities, respectively. A cell-centered finite volume method has been chosen to dicretize the equations by means of the OpenFOAM® open source code [3]. Time integration is performed by means of a second-order backward Euler implicit scheme while convective and diffusive fluxes at the volume faces are evaluated through a second-order central difference scheme. Finally, a pressure-implicit split-operator (PISO) algorithm is used to numerically solve the pressure-velocity coupling. Given the simple geometry of the problem, a structured Cartesian grid is adopted. A laminar free-stream velocity is imposed at the inlet while free-stream boundary conditions (mixed Dirichlet-Neumann conditions) are imposed at the outlet and upper-lower boundaries. Finally, periodic boundary conditions are imposed in the lateral boundaries.

The studied case consists of a flow around a rectangular cylinder whose lengths are $(L_x, L_y, L_z) = (5D, D, 5D)$ at a Reynolds number $Re = 3000$. The extent of the numerical

Case	Δx^+	Δz^+	$N_x \times N_z$	DoF/DoF^{dns}
DNS	6.1	5.4	128×144	1
F1	12.2	10.8	64×72	0.25
F2	12.2	21.6	64×36	0.12
F3	24.4	10.8	32×72	0.12
F4	24.4	21.6	32×36	0.06

Table 1. Parameters of the filtered fields employed for the *a priori* analysis. The values reported of Δx^+ and Δz^+ are averaged in the streamwise directions.

domain is $(\mathcal{D}_x, \mathcal{D}_y, \mathcal{D}_z) = (112D, 50D, 5D)$ and is found to be large enough to not interfere with the flow dynamics, see figure 1. The number of volumes used to discretize the numerical domain is $1.5 \cdot 10^7$ which leads to a near-wall resolution $\overline{\Delta x} = 0.04$, $\Delta y = 0.002$, $\Delta z = 0.034$ where $\overline{(\cdot)}$ denotes the streamwise average along the rectangle length. Although the time integration scheme adopted is implicit, a relatively small constant time step is used, $\Delta t = 0.0023$, which leads to a CFL number less than unity in order to well resolve the small scale unsteadiness of the flow.

3. Filtered fields statistics

In the present section, we assess the behaviour of the LES approach for solving the flow around a rectangular cylinder by means of an *a priori* analysis. The DNS data described in the previous section, are filtered by means of a Gaussian filter,

$$\mathcal{G}_i = \sqrt{\frac{6}{\pi \Delta_i^2}} \exp(-\frac{6 r_i^2}{\Delta_i^2}) \tag{2}$$

so that the resolved field can be written as

$$\bar{u}_i(\mathbf{x}, t) = \int \mathcal{G}_i(\mathbf{x}, \mathbf{x}') u_i(\mathbf{x}', t) d\mathbf{x}' \tag{3}$$

and the subgrid stresses as

$$\tau_{ij}(\mathbf{x}, t) = \overline{u_i u_j} - \bar{u}_i \bar{u}_j \ . \tag{4}$$

In order to analyse the role of the filter length on the resolved and subgrid dynamics, we consider 4 different sets of filter widths as reported in table 1. These sets of filter widths has been chosen to understand the effect of reduction of degrees of freedom to reproduce the flow dynamics and to appreciate the effect of the adoption of a different reduction of resolution in the two horizontal directions. Indeed, from F1 to F4 we have a reduction of computational points with respect to DNS from 0.25 to 0.06, respectively. On the other hand, the filter cases F2 and F3 exploit the same total reduction of degrees of freedom with respect DNS, $DoF/DoF^{dns} = 0.12$ but with different resolutions in the streamwise and spanwise directions. It is worth pointing out that filtering is applied only in the horizontal directions since, the vertical one is commonly recognized to not allow for a significant reduction of the degrees of freedom of the problem when a near-wall resolved LES approach is considered.

To assess the effect of filtering, in figure 2 the iso-contours of the resolved turbulent kinetic energy,

$$q = \frac{1}{2} \langle \bar{u}_i' \bar{u}_i' \rangle \tag{5}$$

are shown. Here, $\langle \cdot \rangle$ denotes the ensemble average and, as customary, the prime denotes fluctuating quantities, i.e. $\bar{u}_i' = \bar{u}_i - \langle \bar{u}_i \rangle$. As expected, the overall effect of filtering is to

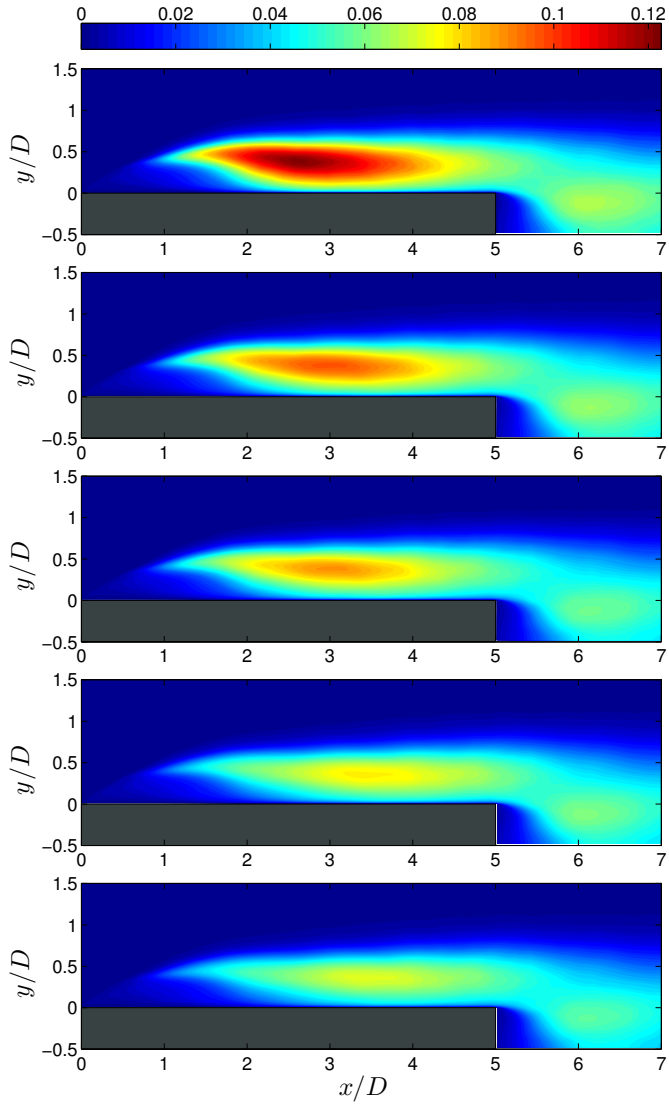

Figure 2. Iso-contours in the $(x-y)$-plane of turbulent kinetic energy. DNS behaviour and the filtering combinations F1, F2, F3 and F4 from top to bottom, respectively.

reduce the amount of resolved energy, see also table 2. In particular, for the F1 case the peak of resolved energy is of the order of 80% the DNS value while for the coarser case F4 is of the order of 59%. Interestingly, the reduction of turbulent kinetic energy is not homogeneous in space thus leading to a modification of the topology of the resolved turbulent intensities. Indeed, moving from F1 to F4 we observe a modification of the shape of the iso-contours and consequently also the position of the maximum intensity is changed. The general trend is a shift towards the wall and in the downstream direction of the region of high turbulence levels, see also table 2. This inhomogeneous effect of filtering is arguably due to the strong inhomogeneity of the flow in terms of spectral distribution of energy, i.e. the energy distribution in the space of scales significantly changes in the different regions of the flow. Hence, the same filter width influences in a different way the energy content in the different regions depending on the amount of energy contained at the small unresolved scales.

From a practical point of view, the *a priori* results shown in figure 2 indicate that the best

Case	q_{max}	$(x/D)_{q_{max}}$	$(y/D)_{q_{max}}$	$q_{max}/q_{max}^{(dns)}$
DNS	0.123	2.57	0.387	1
F1	0.098	2.96	0.383	0.8
F2	0.089	3.07	0.38	0.73
F3	0.078	3.38	0.351	0.63
F4	0.072	3.39	0.35	0.59

Table 2. Scaling of the intensity and position of the peak of turbulent kinetic energy q_{max} as a function of the filter lengths.

compromise between computational costs and reproduction of the main physical processes is the the use of a mesh grid whose resolution is of the order of that of the F2 case. Indeed, we have that the F1 case is certainly able to capture the most energetic flow features but it allows us to reduce the degrees of freedom of the problem to only the 25% those of the DNS. Hence, the mesh properties of the F1 case do not allow for solving this flow at the high Reynolds number regime of the applications. On the contrary, the F4 case allows us to drastically reduce the computational costs being the degrees of freedom of the mesh of the order of 6% those of the DNS. However, the resolved energetics appear to be very poor in terms of both the intensity and the location of the main physical processes. In between these two extreme, the F2 case allows us to reduce the degrees of freedom to the 12% of the DNS and, in the same time, to represent the main physical properties of the flow. It is interesting to point out that the same reduction of the computational costs obtained with a different coarsening in the two wall-parallel directions, as in the F3 case, does not allow to represent the flow features as much with the F2 case.

4. Large Eddy Simulation

Accordingly with the previous results, we perform a Large Eddy Simulation in order to understand if the main outcomes of the *a priori* analysis are confirmed by the *a posteriori* analysis of an actual LES simulation. As anticipated in the introduction, the success of the LES approach is determined not only by the mesh resolution adopted but also by the model for the subgrid stresses used. In the *a priori* analysis shown so far, we considered only the role of the mesh resolution. Actually, the flow around a rectangle and more in general separating and reattaching flows are challenging from a modelling point of view. The reason is given by the simultaneous presence within the flow of laminar, transitional and turbulent regions. These conditions challenge for turbulence models which should be able to switch off when laminar conditions are retained and to smoothly activate when the flow reaches transitional conditions. For these reasons, the choice of the subgrid stress model is of paramount importance when dealing with such kind of flows. Hence, in order to limit our analysis on the effects of resolution, we decide to perform an implicit LES simulation (ILES). This kind of approach consists on resolving the Navier-Stokes equations in a LES grids without the use of an explicit subgrid stress model. The effect of the small unresolved scales is emulated by the numerical dissipation associated with the accuracy of the schemes adopted to solve the equations. This means that the ILES approach automatically predict the laminar regions. Indeed, in the region of the flow where the mesh resolution is fine enough to resolve the flow dynamics the numerical dissipation spontaneously vanishes. Also for these reasons the ILES approach is a good candidate for the present *a posteriori* analysis.

As already demonstrated by several authors, [4, 5], one of the numerical methods particularly prone to perform Implicit Large Eddy Simulations is the Discontinuous Galerkin (DG) method. Indeed, these methods are characterized by a numerical dissipation which mimics the role of

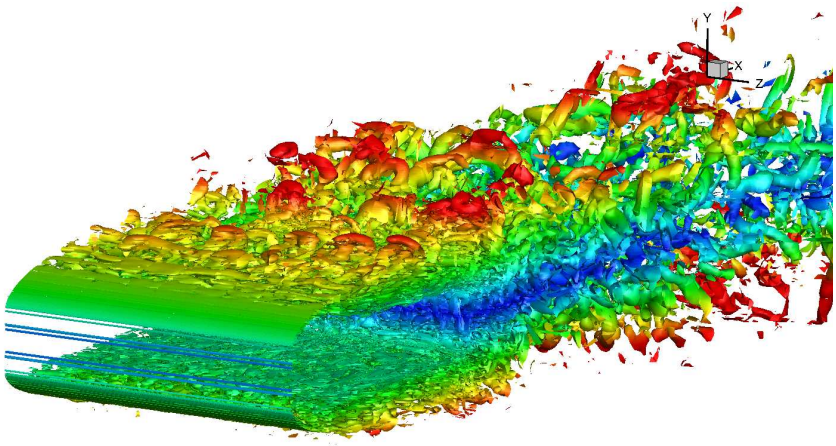

Figure 3. Implicit Large Eddy Simulation of the flow around a rectangular cylinder at $Re = 3000$. Instantaneous iso-surfaces of $\lambda_2 = -1.5$ colored with the distance from the horizontal plane of symmetry of the rectangle.

subgrid-scale models, affecting only the highest wave numbers without spoiling the resolution of the largest resolved scales. It has been also proved [6] that using high order DG discretizations is possible to achieve the same spatial resolution with a reduced number of degrees of freedom (DoF) than standard lower-order methods. In fact, the great geometrical flexibility allows to increase arbitrarily some regions of the fluid domain (for example in the wake of a body) while maintaining very large elements on the farfield.

In this work the DG code MIGALE has been employed to perform the *a posteriori* analysis. The incompressibility constrain is handled through the artificial compressibility flux approach [7], which recovers the hyperbolic nature of the Navier–Stokes equations through a properly modified (only at the mesh element interfaces) Riemann solver, while the viscous numerical fluxes are computed using the BR2 scheme [8]. The simulation has been performed on a computational grid made of 21366 mesh elements using a sixth order polynomial basis. The distribution of the elements and the order of the polynomials are chosen to reproduce the mesh properties of the F2 case shown so far. A Linearly-implicit Rosenbrock-type Runge-Kutta scheme coupled with a low storage matrix-free GMRES solver, preconditioned with a p-multigrid strategy, is used for the time integration. Such high-order implicit scheme allows to integrate efficiently the equations using a large time step size ($\Delta t = 0.05$) without adding sensible numerical dissipation to that of the space discretization.

5. Results of the Implicit Large Eddy Simulation

In this section a preliminary assessment of the Implicit Large Eddy Simulation approach to the flow around a rectangular cylinder is reported. Before addressing the statistics, it is interesting to analyse the instantaneous flow features reproduced by the coarse ILES approach. To this aim we consider the eduction scheme proposed by Jeong et al. [9] which is based on the second largest eigenvalue (λ_2) of the tensor

$$S_{ik}S_{kj} + \Omega_{ik}\Omega_{kj} \tag{6}$$

where

$$S_{ij} = \frac{1}{2}\left(\frac{\partial u_i}{\partial x_j} + \frac{\partial u_j}{\partial x_i}\right)$$

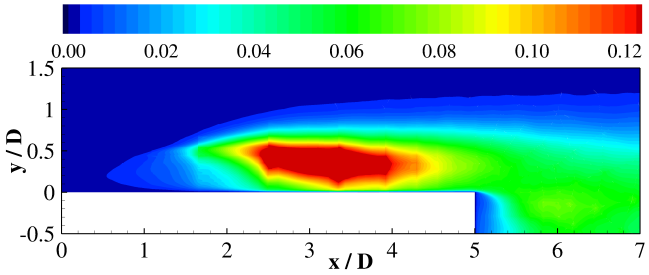

Figure 4. Implicit Large Eddy Simulation of the flow around a rectangular cylinder at $Re = 3000$. Iso-contours in the $(x - y)$-plane of turbulent kinetic energy. The discontinuities observed in the contours are associated with the Discontinuous Glaerkin approach used for the spatial discretization.

$$\Omega_{ij} = \frac{1}{2}\left(\frac{\partial u_i}{\partial x_j} - \frac{\partial u_j}{\partial x_i}\right) \tag{7}$$

are the symmetric and antisymmetric part of the velocity gradient tensor. This eduction scheme is known to accurately extract the three-dimensional pattern of vortical structures.

In figure 3, the instantaneous pattern taken by $\lambda_2 = -1.5$ is shown with iso-surfaces colored by the distance from the horizontal plane of symmetry of the rectangle. It is clear that the main turbulent structures of the flow are captured by the ILES approach. In particular, the development of almost two-dimensional spanwise rolls from the initially laminar leading-edge shear layer as a result of the well-known Kelvin-Helmholtz instability is found to be captured. From these spanwise vortices, the formation of hairpin-like structures [10, 11, 12] is also reproduced. These sparsely distributed structures, grow, burst and decay thus giving rise to a fully turbulent flow.

Let us now address how the ILES approach is able to predict the main energetic features of the flow by considering the behaviour of the turbulent kinetic energy. As shown in figure 4, the distribution of turbulent kinetic energy predicted by the ILES recovers the one of the DNS, see the top plot of figure 2 for comparison. Hence, accordingly with the analysis of the turbulent pattern shown so far, the main transitional and production phenomena of turbulence appear to be correctly reproduced by the ILES simulation. The main difference with respect DNS comes from the intensity of the processes. Indeed, we observe a systematic increase of the intensity of the turbulent fluctuations. As an example the maximum intensity of turbulent kinetic energy reached in DNS is $q_{max} \approx 0.123$ while in the ILES is $q_{max} \approx 0.177$.

6. Conclusions

The flow around a rectangular cylinder is recognized to be challenging for numerical simulations adopting turbulence models as shown by several works in literature, see Bruno et al. [2]. The reason is the simultaneous presence of laminar, transitional and turbulent regions within the flow. Here we try to preliminary assess the behaviour of modelling approaches in such a flow system by addressing first the role of the resolution. To this aim we use Direct Numerical Simulation data to quantify the degree of resolution required to resolve the main physical phenomena of the flow in the context of Large Eddy Simulation. In fact, by filtering the DNS data we defined a good compromise between the need of reduction of computational costs and the need of correctly reproduce the flow physics. In order to prove the effectiveness of the *a priori* results, we performed an actual LES simulation. In particular we implemented an implicit LES in order avoid possible modelling effect on the *a posteriori* results that are intended to focus solely to the effect of the mesh resolution. Indeed, the ILES has been performed by means of

a Discontinuous Galerkin method whose numerical properties are known to be well-suited for ILES. The *a posteriori* results confirm that to reproduce the main physical phenomena of the flow the wall-parallel resolution should be on average of the order of $\Delta x^+ \approx 12$ and $\Delta z^+ \approx 21$ in the streamwise and spanwise directions, respectively.

References

[1] Cimarelli A and De Angelis E 2014 *Phys. Fluids* **26** 055103
[2] Bruno L, Salvetti M V and Ricciardelli F 2014 *J. Wind Eng. Ind. Aerodyn.* **126** 87–106
[3] Weller H, Tabor G, Jasak H and Fureby C 1998 *Comput. Phys.* **12** 620–631
[4] Moura R C, Sherwin S J and Peiró J 2015 *J. Comput. Phys.* **298** 695–710
[5] Bassi F, Botti L, Colombo A, Crivellini A, Ghidoni A and Massa F 2016 *Eur. J. Mech. B-Fluid* **55** 367–379
[6] Chapelier J B, De La Llave Plata M, Renac F and Lamballais E 2014 *Comput. Fluids* **95** 210–226
[7] Bassi F, Crivellini A, Di Pietro D A and Rebay S 2006 *J. Comput. Phys.* **218** 794–815
[8] Bassi F, Crivellini A, Rebay S and Savini M 2005 *Comput. Fluids* **34** 507–540
[9] Jeong J, Hussain F, Schoppa W and Kim J 1997 *J. Fluid Mech.* **332** 185–214
[10] Hourigan K, Thompson M C and Tan B T 2001 *J. Fluids Struct.* **15** 387–398
[11] Langari M and Yang Z 2013 *Phys. Fluids* **25** 074106
[12] Tenaud C, Podvin B, Fraigneau Y and Daru V 2016 *Int. J. Heat Fluid Fl.*